Article

Groundwater Quality Monitoring Using In-Situ Measurements and Hybrid Machine Learning with Empirical Bayesian Kriging Interpolation Method

Delia B. Senoro [1,2,3,4,*], Kevin Lawrence M. de Jesus [2,3,4], Leonel C. Mendoza [4,5], Enya Marie D. Apostol [4,5], Katherine S. Escalona [4,6] and Eduardo B. Chan [7]

1   School of Civil, Environmental and Geological Engineering, Mapua University, Intramuros, Manila 1002, Philippines
2   School of Graduate Studies, Mapua University, Intramuros, Manila 1002, Philippines; klmdejesus@mymail.mapua.edu.ph
3   School of Chemical, Biological, Materials Engineering and Sciences, Mapua University, Intramuros, Manila 1002, Philippines
4   Resiliency and Sustainable Development Center, Yuchengco Innovation Center, Mapua University, Manila 1002, Philippines; lcmendoza@minscat.edu.ph (L.C.M.); emddapostol@minscat.edu.ph (E.M.D.A.); kpsescalona@minscat.edu.ph (K.S.E.)
5   College of Teacher Education, Mindoro State University, Calapan 5200, Oriental Mindoro, Philippines
6   College of Arts and Sciences, Mindoro State University, Victoria 5205, Oriental Mindoro, Philippines
7   Dyson College of Arts and Sciences, Pace University, New York, NY 10038, USA; echan@pace.edu
*   Correspondence: dbsenoro@mapua.edu.ph; Tel.: +63-2-8251-6622

Featured Application: In-Situ and Hybrid Machine Learning—Geostatistical Interpolation method for groundwater quality monitoring applications.

Abstract: This article discusses the assessment of groundwater quality using a hybrid technique that would aid in the convenience of groundwater (GW) quality monitoring. Twenty eight (28) GW samples representing 62 barangays in Calapan City, Oriental Mindoro, Philippines were analyzed for their physicochemical characteristics and heavy metal (HM) concentrations. The 28 GW samples were collected at suburban sites identified by the coordinates produced by Global Positioning System Montana 680. The analysis of heavy metal concentrations was conducted onsite using portable handheld X-Ray Fluorescence (pXRF) Spectrometry. Hybrid machine learning—geostatistical interpolation (MLGI) method, specific to neural network particle swarm optimization with Empirical Bayesian Kriging (NN-PSO+EBK), was employed for data integration, GW quality spatial assessment and monitoring. Spatial map of metals concentration was produced using the NN-PSO-EBK. Another, spot map was created for observed metals concentration and was compared to the spatial maps. Results showed that the created maps recorded significant results based on its MSEs with values such as 1.404×10^{-4}, 5.42×10^{-5}, 6.26×10^{-4}, 3.7×10^{-6}, 4.141×10^{-4} for Ba, Cu, Fe, Mn, Zn, respectively. Also, cross-validation of the observed and predicted values resulted to R values range within 0.934–0.994 which means almost accurate. Based on these results, it can be stated that the technique is efficient for groundwater quality monitoring. Utilization of this technique could be useful in regular and efficient GW quality monitoring.

Keywords: groundwater; heavy metals; physicochemical parameters; in-situ; machine learning; geostatistical analysis

1. Introduction

Water quality is associated with ecosystem preservation, economic growth and social development [1]. Groundwater (GW) quality is critical to the Philippines' overall water resource; hence, monitoring should be given attention. Population expansion and the acceleration of modernization as well as industrialization have resulted in an increased

water demand [2]. It is inevitable that quality of both surface water and GW is compromised in areas where economy is in transition and where there is increasing urbanization, industrialization, and agricultural activities [3]. However, due to scarcity of elemental laboratory instruments in the Philippines, the preparation requirements of the laboratory station-based instruments for samples, and the travel time from sampling sites to laboratory stations become a challenge to GW quality monitoring especially to elemental concentration analysis.

The population of the Philippines has rice in its regular daily meals. Rice fields and techniques to produce high and good quality yields are among the agricultural areas and programs, respectively, that are being supported by the Philippine government. Calapan City, Oriental Mindoro province in the Philippines, with GW as primary water source, is among the top producers of rice in the country. Rice fields require highly flattened area and good water quality as among the criteria to increase yields with good rice quality. Having the Philippines within the tropical storm belt, Calapan City experienced regular flooding as shown in Figure 1. This condition become a challenge to the water quality for rice fields and for domestic supply.
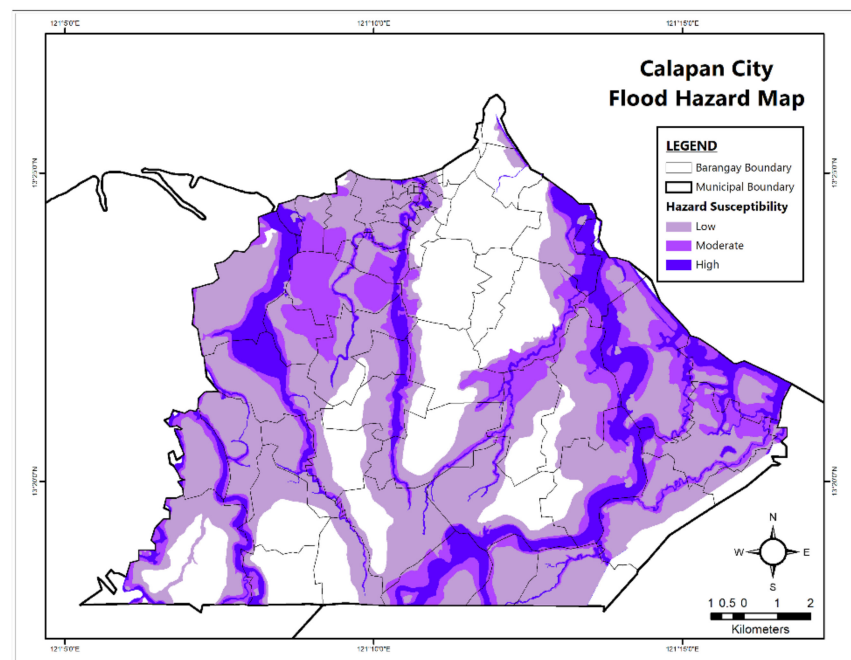
Figure 1. Flood Hazard Map of Calapan City [4].

The Philippines is rich in natural resources such as metals and non-metallic minerals [5] with tropical climate where annual rainfall is high. However, anthropogenic activities, due to economic development, population positive growth rate and urbanization, caused unintentional adverse effects to the environment. When the pristine environment is disturbed, and minerals are exposed to oxygen and water, chemical reactions happen. Similar condition takes place during weathering. Having rich in mineral resources, high annual rainfall, large flattened agricultural areas, and GW as primary source of water supply, GW quality monitoring is important. Water quality that has elevated concentration of metals such as arsenic (As), copper (Cu), iron (Fe) nickel (Ni), manganese (Mn), lead (Pb), and other metals known for its toxicity characteristics would have acute and/or chronic adverse effects to human health [6–8].

Several technologies for measurement of the presence of metals in GW exists such as Inductively Coupled Plasma—Mass Spectrometry (ICP—MS), Inductively Coupled Plasma—Optical Emission Spectrometry (ICP—OES), and Atomic Absorption Spectrometry (AAS). These approaches are laboratory-based and require several days before result

of analysis is available. This condition become not suitable for field monitoring and measurements [9] in sub-urban, rural areas, areas where access is a challenge and when time is a primary criterion in the analysis. These conditions require in-situ measurements, and accurate detection become a critical component in monitoring the GW quality. In-situ measurements provide observations on a rapid phase as well as covering the wider areas especially those with difficulty in access. This is in contrast of laboratory—based methods with significant limitations such as expensive instrumentation making limited availability, complex sample preparation and applicability in field conditions [10]. There are on-site detection and monitoring techniques such as electrochemical analysis [10,11], cyclic voltammetry (CV) [12], anodic stripping voltammetry (ASV) [13], square wave anodic stripping voltammetry (SWASV) [14], electro-chemical impedance spectroscopy (EIS) [15], electrochemiluminescence (ECL) [16] and the use of piezoelectric biosensors [17]. However, these techniques have drawbacks such as background noise control, unable to fulfill the current requirements for selectivity [9], detection limits of CV [12], insolubility of metals and the multiple peaks of ASV [13], complicated interferences and complex matrices in SWASV [14], EIS's inability to identify different ions [15], frequent fouling of electrodes in the case of ECL [16], and only few enzymes are sensitive to heavy metals for the case of biosensors [17]. Hence, the use of portable x-ray fluorescence spectrometry (pXRF) technique in onsite metals detection and analysis is appropriate in rugged condition yet provides user of accurate and rapid analysis. This is in contrast of laboratory-based methods with significant limitations such as expensive instrumentation, complex sample preparation and applicability in field conditions [18]. Therefore, non-destructive analytical technique, such as relatively simple spectra line void of many interferences and rapid multi-element analyses [19], contributes significantly to the successful implementation of this study.

Concentration maps were frequently used tool for spatial monitoring. Spatial information in water resources are limited, and GW quality data can be obtained only through spot sampling. However, this procedure often requires extensive manpower and resources [10]. The issue in this practice and the determination of sample locations density influences the accuracy of the generated spatial maps [19]. The integration of in–situ measurements and GIS—based spatial interpolation techniques offer an improvement in the presentation and display of the status of GW quality in an area. The use of this integrated approach provides a clear and intelligent base—maps which can be utilized by researchers, policy makers, implementors for planning proposals [20] and creation of strategic programs.

Several studies on GW monitoring and assessment implemented using GIS—based approaches focused on different Southeast Asian countries such as the Philippines [1,21], Thailand [22], Malaysia [23], Singapore [24], Indonesia [25], Cambodia [26], Laos [27], and Vietnam [28]. This article illustrates the quantification and mapping of the concentrations of heavy metals such as Ba, Cu, Fe, Mn, and Zn in GW and presents the utilization of in-situ GW quality monitoring that uses a hybrid machine learning-geospatial interpolation technique and pXRF. This type of technique and analyses give prompt, accurate data and information on the current GW quality. This is to address the challenges encountered on-ground during sampling activities, the scarcity of instruments in the Philippines due to its price, and the complex samples preparation required by some laboratory-based instruments. Analyzing heavy metal concentrations in a faster, accurate and convenient method can help the researchers, authorities, water utility companies and local government units in making prompt decision, guidelines and strategic programs.

2. Materials and Methods

2.1. Description of the Study Area

The study area is Calapan City, in the province of Oriental Mindoro, Philippines. This is a third-class city and one of only two cities in the MIMAROPA region of the Philippines. It is the capital of the island province of Mindoro and located on the island's northeastern shore. It has a population of about 150,000 people (about 25,000 households)

and 62 barangays (the smallest local government unit) [29]. The city lies within 13°22′ N Latitude and 121°9′ E Longitude and Mindoro is located approximately 13°11′ N Latitude and 121°53′ E Longitude south of Mainland Luzon. The island of Mindoro is popularly known of rice production. Calapan City has an area of 217.30 square kilometers. Deep and shallow wells, in addition to piped water supply, are currently the primary sources of water in the city.

2.2. Collection/Treatment of Groundwater Samples

The GW samples were collected from twenty-eight (28) suburban deep and shallow well sites following the USEPA SESDPROC-301-R3/SESDPROC-111-R4 [30] as shown in Figure 2. The GW samples were collected using stainless steel sampler and polyethylene (PE) bottles. The PE bottles were thoroughly pre-washed with Type 1 water. Each PE bottle was carefully labeled, sealed, and placed temporarily in coolers for metals concentration detection. This is in preparation for the detection of the presence of metals concentration in all collected GW samples.
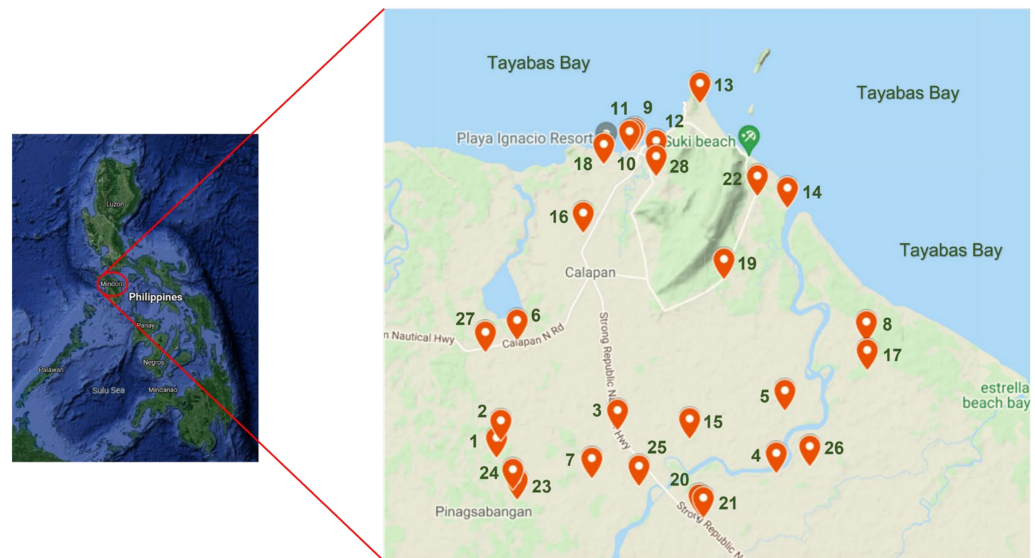
Figure 2. Map of the Study Area and Sampling Sites.

2.3. Physicochemical and Metal Concentrations Analysis

Temperature, pH, electric conductivity (EC), and total dissolved solids (TDS) of the samples were determined onsite using a multi-parameter water analyzer (HANNA HI 9811-5) with HI1285-5 probe (electrode) and HI7007, HI70031, HI70032, buffer solutions for calibration [31]. The HI7007, HI70031, HI70032 solution were used for pH, EC and TDS calibration, respectively. While HI700661 solution was used for cleaning the electrode. The physicochemical values detected in groundwater were compared to the permissible limits specified in the 2017 Philippine National Standards for Drinking Water (PNSDW) [32] and the WHO Drinking Water Guidelines [33,34]. These water parameters were used in the hybrid machine learning technique.

The heavy metal concentration analysis employed the use of portable handheld Olympus Vanta X-Ray Fluorescence Spectrometry. This pXRF is a rapid onsite accurate elemental analyzer that could be used for various environmental media including water [35–39]. The pXRF was set on geochem mode and recorded metals concentration in ppm (mg/L) detected from GW samples. Target metals were Ba, Cu, Fe, Mn and Zn.

2.4. Spatial Concentration Mapping Using Machine Learning Informed Empirical Bayesian Kriging (EBK) Method

Hybrid machine learning—geostatistical interpolation (MLGI) method was employed. The EBK technique was used to produce spatial concentration maps of the GW's physicochemical properties and heavy metal concentrations. By sub-setting and replicating observed data, the EBK automates the most time-consuming aspects of constructing a viable kriging model. EBK provides a distribution of semi-variogram models and compensates for semi-variogram estimate uncertainty. The EBK is more realistic and superior to other current geostatistical modeling methods owing to its dependence on limited maximum likelihood estimation. This is in contrast to other existing kriging models that rely on weighted least squares estimation. EBK has many significant benefits, including a low need for interactive modeling, more accurate prediction of standard error and projection for small datasets as compared to other traditional kriging techniques, and exact prediction of substantially non-static data [40].

The Artificial Neural Network (ANN) approach is a subset of methods for artificial intelligence inspired by biological neurons. It is capable of quickly acquiring patterns and forecasting the result of a problem in a multi-dimensional environment. ANN models are trained using datasets [41] to show the efficacy. The training algorithm and the transfer function that was utilized in the model are two critical components of the ANN model. The Levenberg—Marquardt (LM) algorithm was chosen as the training algorithm since it is the quickest function for training a network, and the hyperbolic tangent sigmoid function was used as the transfer function because it is the recommended transfer function for rapid processes [42,43].

Particle Swarm Optimization (PSO) is a population-based stochastic optimization technique inspired by biological communities' collaborative nature. The PSO is initiated using a community of randomly generated particles as solution options. It looks for global optima via iterations in which particles with their own velocity fly around the search space following the current optimum particles, which is the best approach for finding the best solution. The PSO was integrated to the ANN to determine the weights and biases which gives the minimum error [44].

This hybrid technique integrated to the EBK method generated the spatial concentration maps of the target study area. The Neural Network—Particle Swarm Optimization (NN-PSO) approach was applied to generate the spatial concentration maps of physicochemical parameters and HM concentrations.

3. Results

Subsequent sections elaborate the results of the study and in comparison, of the WHO and PNSDW guidelines.

3.1. Physicochemical Groundwater Parameters

The recorded physical and chemical properties of groundwater of the 28 sampling points are shown in Table 1, and in comparison to WHO (2017) and PNSDW (2017) guidelines. The detailed description of the sampling locations of the study area with the physicochemical properties of GW were exhibited in Table A1 of Appendix A.

Table 1. The groundwater physical and chemical properties.

Sampling No.	Temperature (°C)	pH	EC (μS/cm)	TDS (ppm)
1	28.3	7.9	130	60
2	28.5	8.4	130	60
3	26.2	8.5	120	50
4	29.2	7.6	660	320
5	30.7	7.8	1200	590
6	27.1	8.8	130	50
7	27.2	7.9	200	90
8	32.4	7.1	900	440
9	31.6	7.5	350	160
10	32.5	7.5	970	480
11	31.4	7.4	1820	900
12	31.1	7.1	780	380
13	31.0	7.0	990	490
14	32.0	7.5	600	290
15	28.1	7.5	220	100
16	31.5	7.3	570	270
17	30.6	7.3	820	400
18	29.2	8.1	690	340
19	30.2	7.4	410	200
20	30.1	7.6	140	160
21	28.4	8.3	180	150
22	33.6	7.7	910	450
23	28.7	8.3	140	60
24	27.4	8.4	140	60
25	32.9	7.6	750	370
26	29.7	7.3	500	240
27	29.7	7.7	100	40
28	30.3	6.7	1140	560
WHO [45]	30.0	6.5–8.5	400	1000
PNSDW [46]		6.5–8.5	-	600

The GW temperatures ranged from 26.2 to 33.6 degree Celsius which could lead to increased release rates of metals concentration especially within the water temperature of 30–35 degrees Celsius [47]. Furthermore, the study of Zhu, et al. in 2010 [48] attributed the high temperature in GW to the boom of urbanization that was also observed in the City of Calapan. The recorded pH of GW ranged from 6.7 to 8.8 which is within the pH range guidelines set by the WHO and PNSDW [49]. The release rates of metals were affected by a lower water pH. Lower pH of water means acidic water and known to be aggressive, enhancing the breakdown of Fe and Mn resulting in an unpleasant taste in water [50]. This condition could have adverse effects including heavy metal poisoning and toxicity [51–53]. The majority of the water samples are slightly basic which could be attributed to the existence of carbonates and bicarbonates [54]. The TDS and EC range recorded was 40–900 ppm and 100–1820 μS/cm, respectively. The TDS in GW found to be below WHO guidelines; however, beyond PNSDW guidelines. The TDS and EC had been found to have positive correlation [55]. The elevated EC of 1820 μS/cm has been attributed to inorganic chemicals in ionized form in water [54] such as metal elements.

3.2. Heavy Metal Concentrations

Presence of heavy metals were investigated in GW samples collected from the 28 sampling sites as indicated in Figure 2. Detected concentrations were compared to the existing maximum allowable limit of the WHO and the PNSDW 2017. These limits are enumerated in Table 2. The toxicants found in the GW samples are discussed in more detail in the subsections below.

Table 2. Permissible limits of metals in groundwater.

Parameter, mg/L	WHO	USEPA (2009)	PNSDW 2017
Ba	0.7 [56]	2.00	0.70
Cu	1.30 [45]	1.30	1.00
Fe	-	0.30	1.00
Mn	0.40 [1]	0.05	0.40
Zn	-	5.00	-

[1] Guidance value.

3.2.1. Barium

All sampling locations observed Ba concentrations below permissible limits (Figure 3) of WHO, USEPA and PNSDW. The presence of Ba in GW has been attributed to the weathering of rocks such as igneous rocks, sandstone, shale, and coal [57,58].
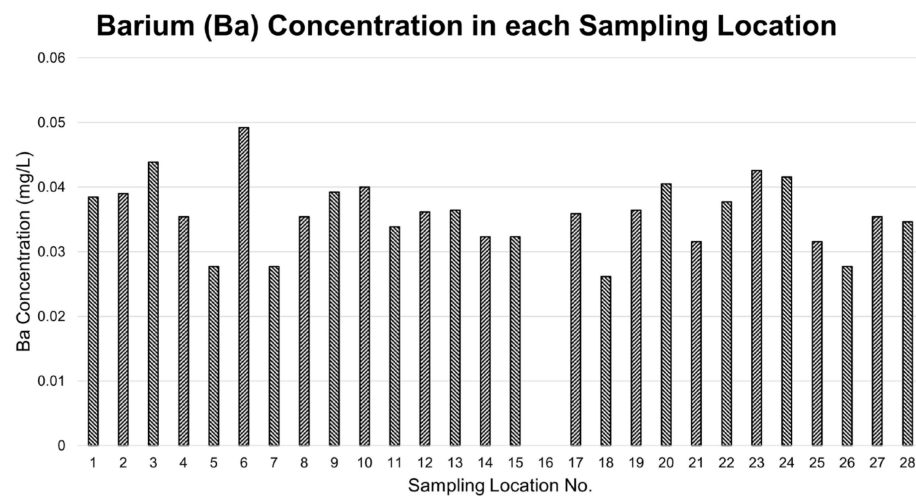
Figure 3. Concentration of Ba in GW samples.

3.2.2. Copper

The Cu concentrations (Figure 4) in GW samples from all sampling locations did not exceed the WHO guideline of 1.3 mg/L. The Cu in trace amounts in GW was associated to the kind of rock that forms the aquifer [59]. Another possible source of copper is the pipeline. Also, Cu concentrations at all sampling sites were within the acceptable limit of PNSDW (1 mg/L) and WHO guidelines.
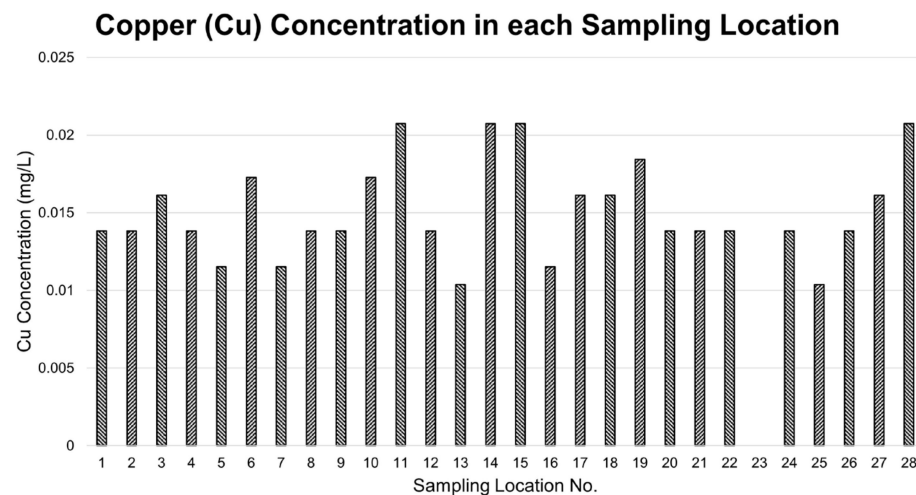
Figure 4. Concentration of Cu in GW samples.

3.2.3. Iron

Iron stains laundry and plumbing fixtures at concentrations more than 0.3 mg/L; it can also give metallic taste [60]. Hence, USEPA set an allowable concentration limit of 0.3 mg/L. The majority of the Fe in GW comes from minerals and sediments which may be in the form of particulate or dissolved [61]. The Fe concentration in each sampling location is presented in Figure 5. Sampling location 8 recorded an elevated Fe concentration. This was attributed to a longer residence time [62] which is associated to the type of subsurface (aquifer) that promotes longer residence time and creates opportunity for metals to react through chemical and physical weathering [63]. In addition, the area shown in Figure 2 illustrates the area of sampling point 8 of having lesser active wells. This condition also contributes to longer residence time of GW.
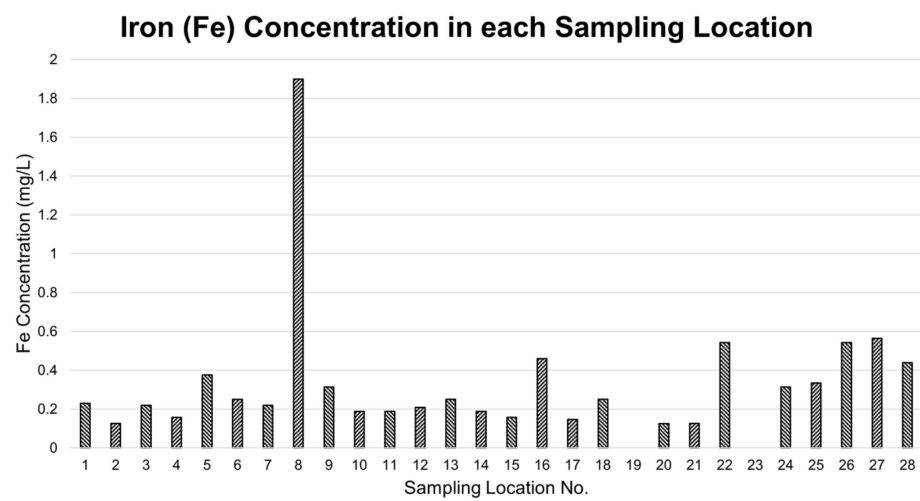
Figure 5. Concentration of Fe in GW samples.

3.2.4. Manganese

Groundwater samples collected from all sampling locations did not exceed the WHO's maximum permissible level for Mn concentration (Figure 6). The natural occurrence of Mn in GW can be influenced by several factors including TDS, GW level fluctuations, and the residence time. Agricultural operations and domestic wastewater are additional potential two sources of Mn that can adversely affect the GW quality [64,65].
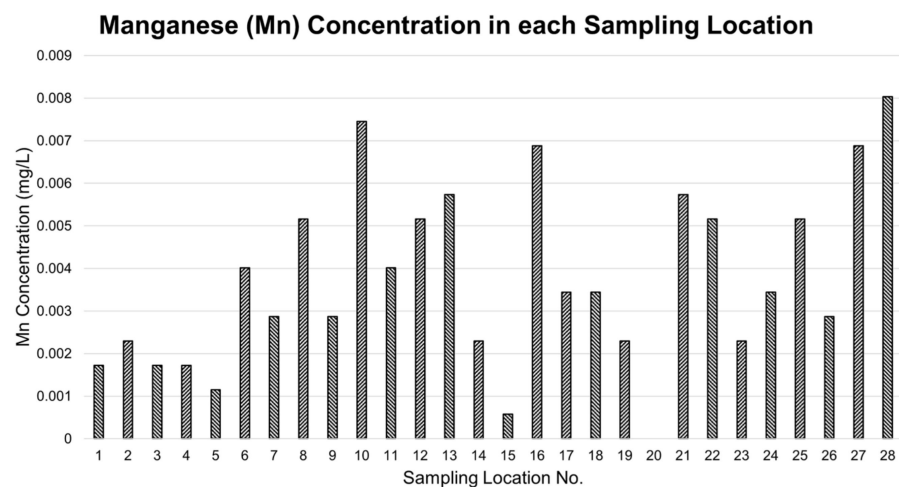
Figure 6. Concentration of Mn in GW samples.

3.2.5. Zinc

The highest concentration of Zn was recorded at Brgy. Gutad. However, this highest Zn concentration was within the WHO and PNSDW permissible limits. Several locations observed without Zn concentrations were at Brgy. Balingayan, Brgy. Maidlang, Brgy. Managpi, and Brgy. Personas. Zinc is naturally found in GW and the acidity affects the quality [64]; hence, it is important that monitoring is carried out. The acidity theory states that the higher the acidity (i.e., lower pH) of the water, the higher the Zn concentration. As observed in Table 1, GW samples from all sampling sites were slightly basic which explains the low concentration levels of Zn. The Zn concentration in each sampling location is presented in Figure 7.
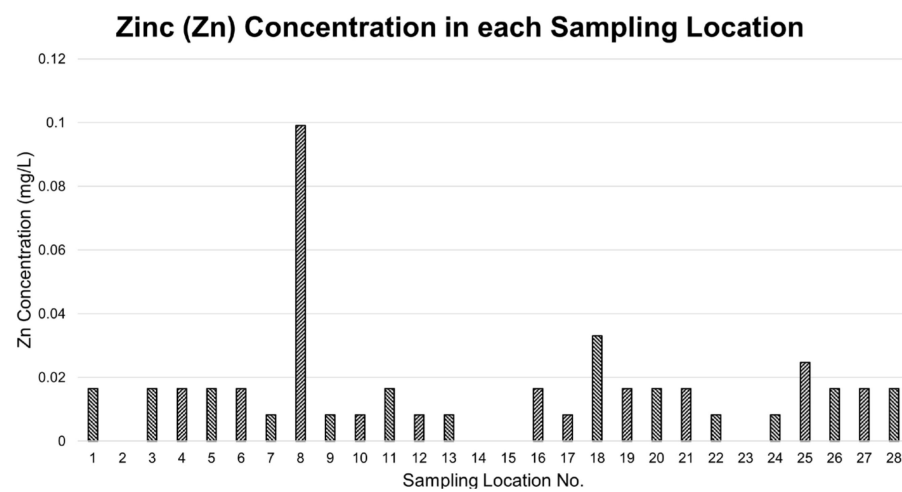
Figure 7. Concentration of Zn in GW samples.

3.3. Correlation Analysis

The correlations between the physicochemical characteristics were investigated using Pearson correlation analysis calculated through International Business Machine Statistical Package for Social Sciences (IBM SPSS). The r and p values were presented. The r value expresses the relationship between variables. The p value expresses the significance of the relationship. A lower *p*-value denotes statistical significance, whereas a higher *p*-value denotes the opposite. A negative correlation was found between pH and the other variables, while a positive correlation was found between the other parameters. At the 0.01 p level, all relationships were significant. The correlation matrix for the physicochemical parameters are presented in Table 3.

Table 3. Correlation matrix of the physicochemical parameters.

Parameter	Temp	pH	EC	TDS
Temp	1.000			
pH	−0.665 **	1.000		
EC	0.657 **	−0.602 **	1.000	
TDS	0.664 **	−0.603 **	0.995 **	1.000

** Correlation is significant at the 0.01 level (2-tailed).

A substantial negative correlation was observed between pH and temperature (r = −0.665), pH and EC (r = −0.602), and pH and TDS (r = −0.603) which is similar to the findings of Abou Zakhem et al. in 2017 [66] and Sunkari and Abu in 2019 [67]. On the other hand, a substantial positive correlation was observed between temperature and EC (r = 0.657), temperature and TDS (r = 0.664), and EC and TDS (r = 0.995). This correlation values agreed to the findings of Wali et al. in 2021 [68].

Similar to physicochemical parameters, Pearson correlation analysis for the relationships between Ba, Cu, Fe, Mn, and Zn was also taken. Fe was positively correlated with Mn and Zn; and Mn was positively correlated with Zn. Positive substantial correlations between these metals indicated the same origin, are mutually dependent, and have similar transport characteristics [69]. The positive p with higher r values of this study illustrates relationship between metals; however, this relationship was not significant. The presence of these metals in GW is attributed to natural weathering of rocks. The correlation matrix for metals concentrations is shown in Table 4.

Table 4. Correlation matrix for the heavy metal concentration of groundwater samples.

Metal	Ba	Cu	Fe	Mn	Zn
Ba	1				
Cu	0.055	1			
Fe	−0.136	−0.001	1		
Mn	−0.235	0.072	0.320	1	
Zn	−0.089	0.013	0.870 **	0.190	1

** Correlation is significant at the 0.01 level (2-tailed).

3.4. Spatial Concentration Mapping Using NN-PSO + EBK

The NN-PSO simulation was applied to accelerate the performance of the prediction capability of the EBK method. The simulation showed an excellent result as evident to the mean squared error (MSE) and correlation coefficient (R) values wherein the ideal value is 0 and 1, respectively. The NN-PSO simulation performed for the physicochemical parameters and heavy metal concentrations are presented in Table 5. Correlation plots of the R (validation) and R (testing) for the governing NN-PSO models of physicochemical parameters and heavy metals concentration are illustrated as Figure A1 of Appendix B.

Table 5. NN-PSO Simulation Results.

	Hidden Neurons	No. of Particles	No. of Iterations	Elapsed Time (sec)	MSE	R Validation	Testing
Temp	25	3	2000	180.38559	0.01204	0.99878	0.99656
pH	29	10	2000	119.16085	0.00434	0.99078	0.99039
EC	30	1	2000	163.34882	0.00155	0.99851	0.99966
TDS	27	3	2000	337.90592	0.00032	0.99925	0.99981
Ba	29	1	2000	172.62202	2.44×10^{-6}	0.98838	0.99286
Cu	29	3	2000	366.12861	1.64×10^{-7}	0.99826	0.99636
Fe	28	3	2000	139.78693	0.00091	0.99010	0.99951
Mn	29	5	2000	115.26285	1.34×10^{-7}	0.98252	0.99725
Zn	30	1	2000	142.60618	1.08×10^{-5}	0.97945	0.99580

The relationship between the number of neurons ranging from 1 to 30 and the corresponding AIC (Akaike Information Criterion) values obtained for the physicochemical parameters (temperature, pH, EC, and TDS) as well as the heavy metal concentrations are exhibited in Figures 8 and 9, respectively. These figures represent the AIC values of all NN-PSO models for each hidden neuron that was simulated in this study. It was observed that the best models for the physicochemical parameters were determined from the 25, 29, 30, and 27 hidden neurons (HN) for temperature, pH, EC and TDS, respectively. The best models for Ba, Cu, Fe, Mn, and Zn were observed in 29, 29, 28, 29, 30 HN, respectively, for the heave metal concentrations.
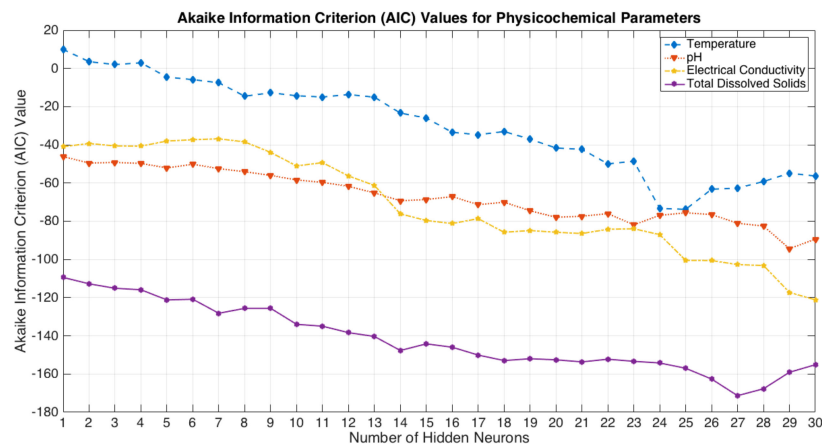
Figure 8. The AIC Values for Physicochemical Parameters.
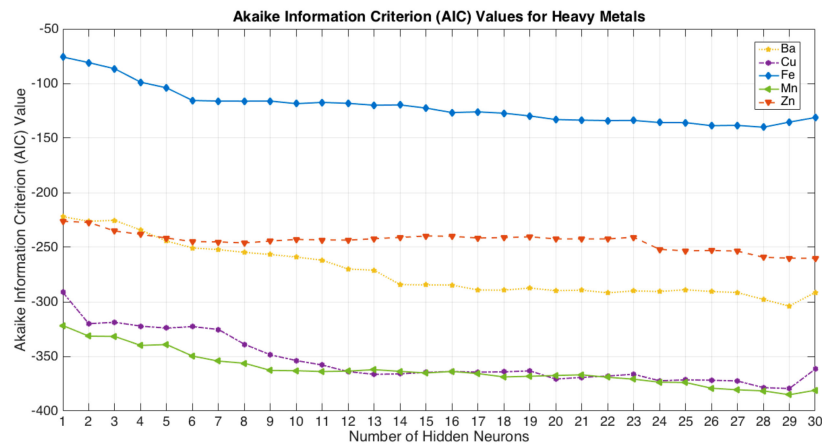
Figure 9. The AIC Values for Heavy Metals.

The spatial concentration of the physicochemical parameters of GW in Calapan City, Oriental Mindoro was mapped using NN-PSO+EBK interpolation method. The highest temperature for GW recorded in the study area was 33.6 °C which was observed in Brgy. Parang. While the least temperature was observed in Brgy. Biga with recorded temperature of 26.2 °C. The highest pH for GW was observed at Brgy. Canubing I, with pH equal to 8.8. The lowest pH was detected at Brgy. Sto. Nino with pH of 6.7. The highest EC and TDS observed in Brgy. Ibaba West with EC and TDS value of 1820 μS/cm and 900 ppm, respectively. The least observed EC and TDS concentration was 100 μS/cm and 40 ppm, respectively which was recorded in Brgy. Sta. Rita. The spatial concentration of the physicochemical parameters of GW is shown in Figure 10.
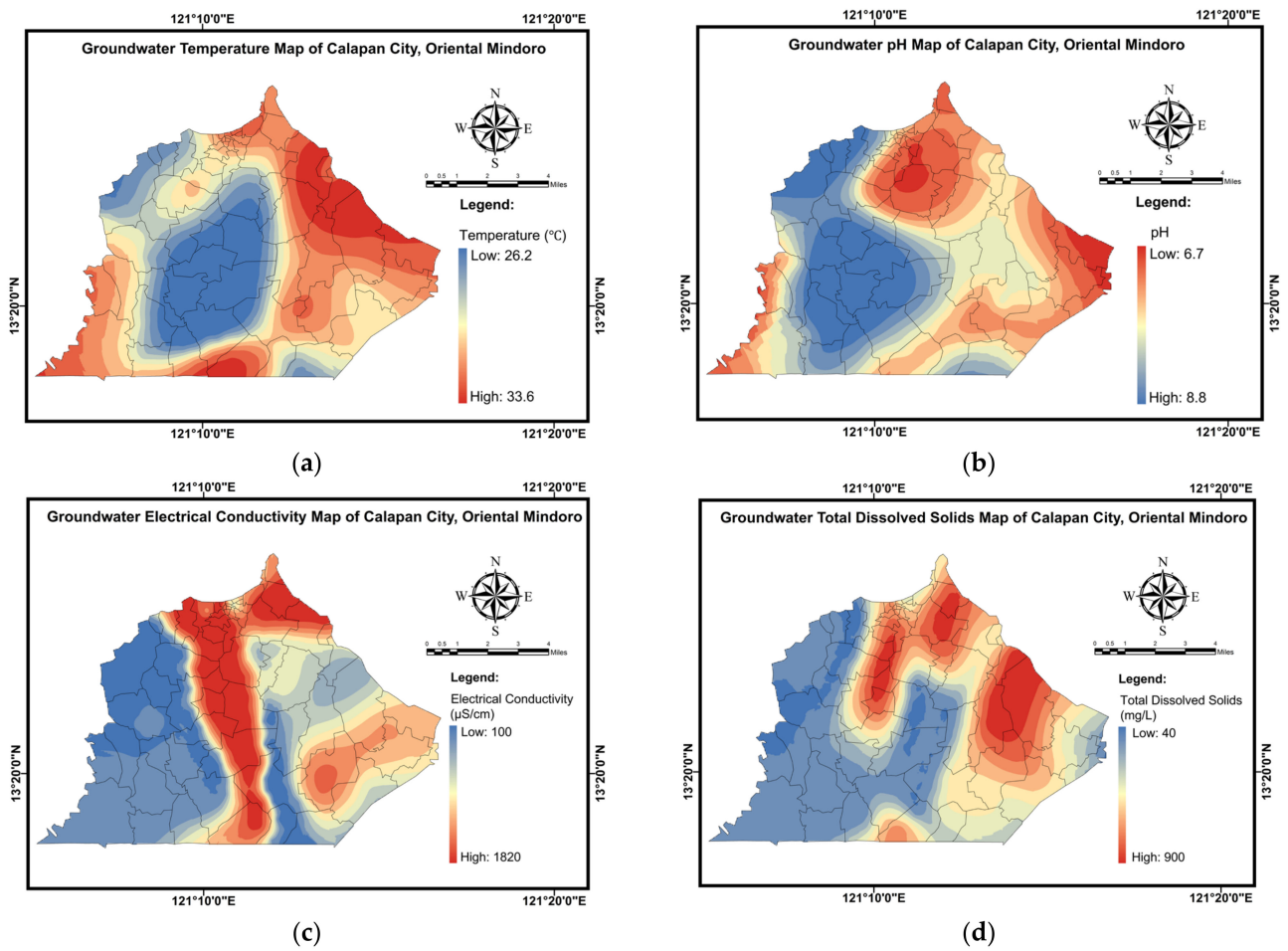
Figure 10. Physicochemical parameters map of Calapan City (**a**) Temperature, (**b**) pH, (**c**) EC, and (**d**) TDS.

The spatial concentration of the heavy metals of GW in Calapan City, Oriental Mindoro including Ba, Cu, Fe, Mn, and Zn was also mapped using the NN-PSO+EBK interpolation method. The heavy metal concentration maps generated using the NN-PSO+EBK method was presented in Figure 11.
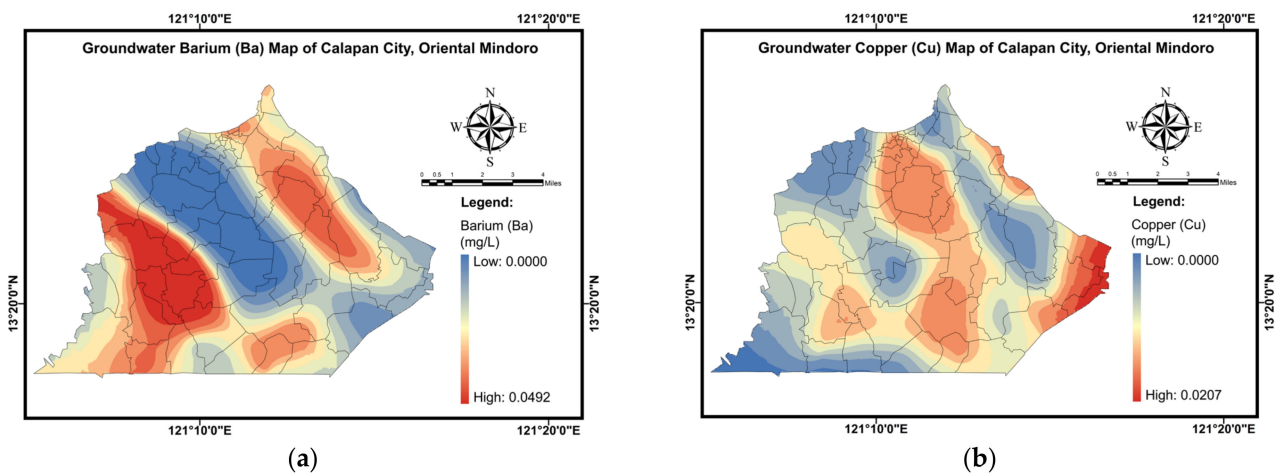
Figure 11. *Cont.*
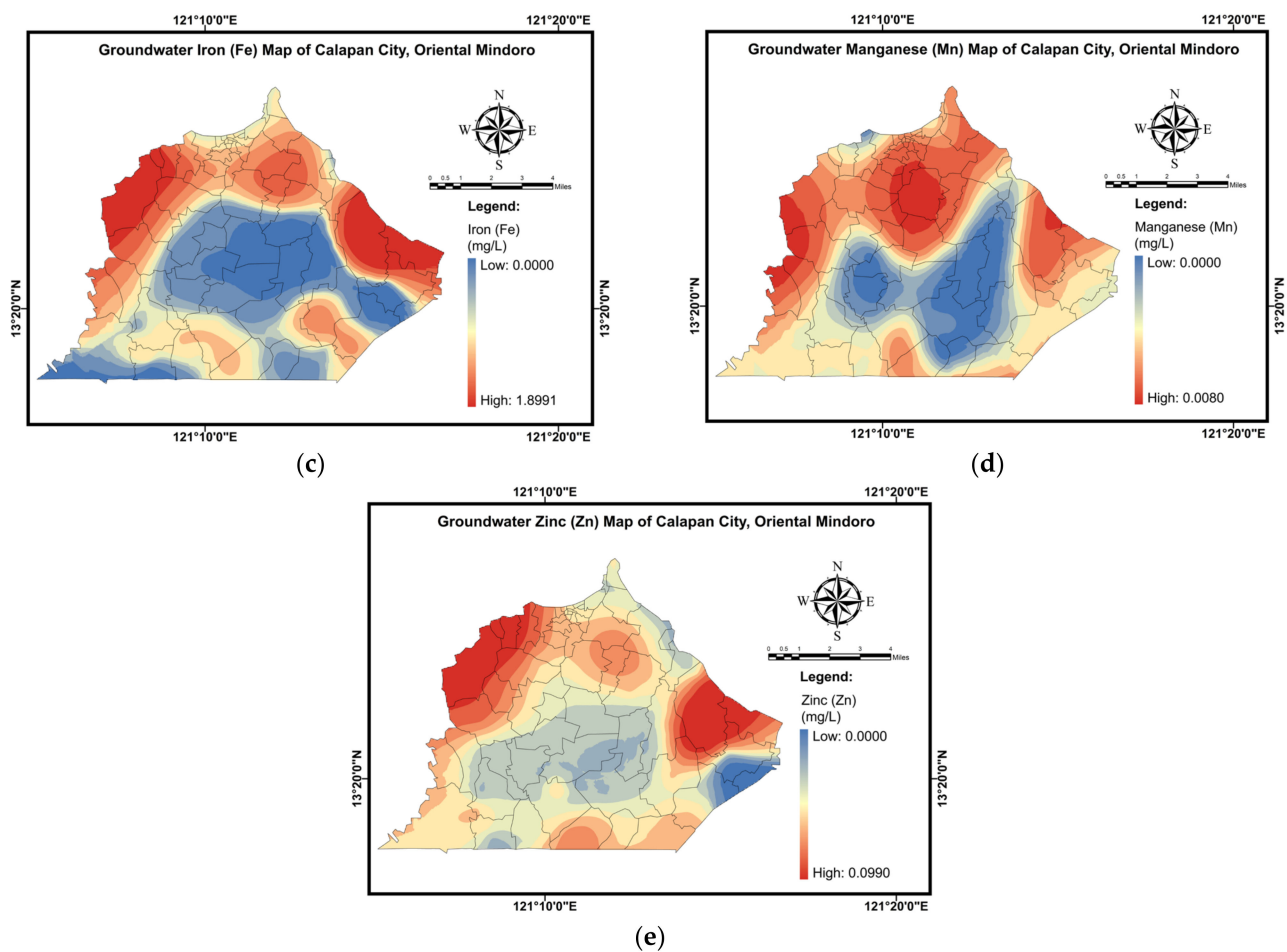
Figure 11. Heavy metal concentration map of Calapan City (**a**) Ba, (**b**) Cu, (**c**) Fe, (**d**) Mn, and (**e**) Zn.

The highest Ba concentration was measured in Brgy. Canubing I, where it was 7.9 times more than the background value for Ba measured in the research area. The average Ba concentration across all sample sites was 5.6 times more than the background value in the area of study. The highest concentrations of Cu were measured at several locations and recorded to be three times greater than the background concentration of copper. The mean concentration of Cu was found to be 2.1 times that of the background concentration. The Fe concentrations were found to be highest in Brgy. Gutad where it was found to be 6.1 times greater than the background value reported for the research region. Moreover, multiple sites were observed to exceed the WHO standards for Fe. These sites include Brgy. Camansihan, Brgy. Ibaba East, Brgy. Masipit, Brgy. Parang, Site 2 of Brgy. Personas, Brgy. San Vicente East, Brgy. Sta. Cruz, Brgy. Sta. Rita, and Brgy. Sto. Nino. Meanwhile, the mean concentration in Calapan City was just 0.5 percent more than the background level. Mn and Zn concentrations were highest in Brgy. Sto. Nino and Brgy. Gutad, respectively. However, these concentrations were still below the background concentration in the research region. The heavy metal concentration trend in the study area was observed to be Mn < Cu < Ba < Zn < Fe. Generally, these concentrations are within the WHO, USEPA and PNSDW limit except for Fe in several areas.

3.5. Cross Validation and Spot Sampling Evaluation Results

The predicted and observed values were compared to the NN-PSO+EBK method using the correctness measures to test the robustness of the predicted models. The results shown in Table 6 exhibit a robust and accurate result based on the R values close to 1. The cross-validation results suggested that all values provided more accurate spatial distribution for the study area. The cross-validation results are presented in Table 6.

Table 6. Cross Validation Results for NN-PSO+EBK simulation.

Criteria	Temp	pH	EC	TDS	Ba	Cu	Fe	Mn	Zn
R	0.989	0.990	0.934	0.977	0.994	0.976	0.985	0.975	0.984

A spot sampling analysis was performed using the data from the households in different barangays of Calapan City. A total of 21,559 households were utilized in the spot sampling analysis which is presented in Figure 12. The distribution of the households included in the spot sampling analysis per barangay is presented in Figure 13.
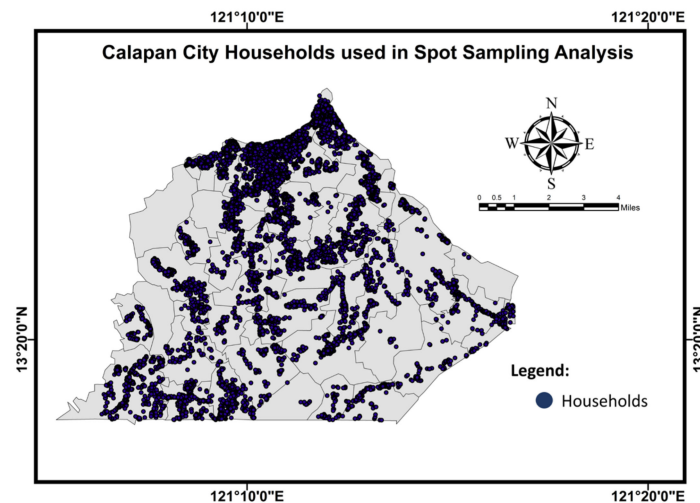
Figure 12. Concentration of Zn in GW samples.
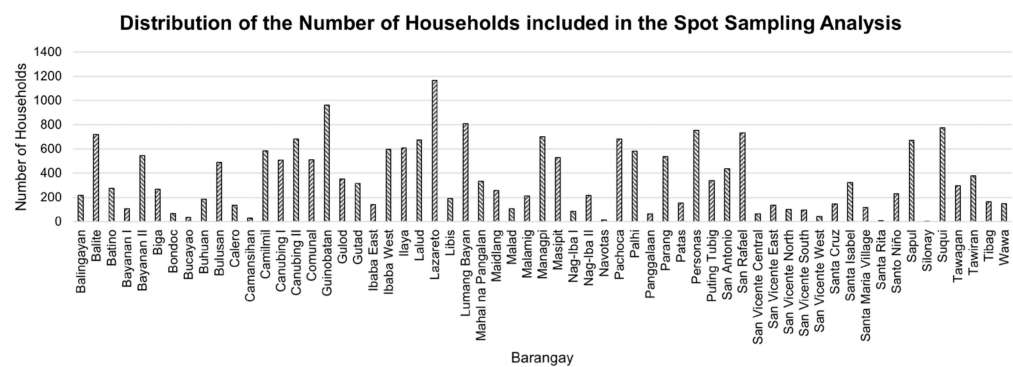
Figure 13. Distribution of the Number of Households included in the Spot Sampling Analysis.

The spot sampling results was compared to the spatial concentration maps created in Figure 11. Table 7 exhibits the spot sampling comparison results for all heavy metals detected in the GW resources in Calapan City. The results showed that the created maps provided good results based on its MSE which is approaching zero when contrasted to the spot sampling values.

Table 7. Spot Sampling Comparison Results.

Criteria	Ba	Cu	Fe	Mn	Zn
MSE	0.0001404	0.0000542	0.0006260	0.0000037	0.0004141

Considering each barangay, the MSEs for each element were also obtained as presented in Table A2 of Appendix C. Figure 14 presents the summary of the spot sampling comparison results in each barangay for all heavy metals considered in the study.
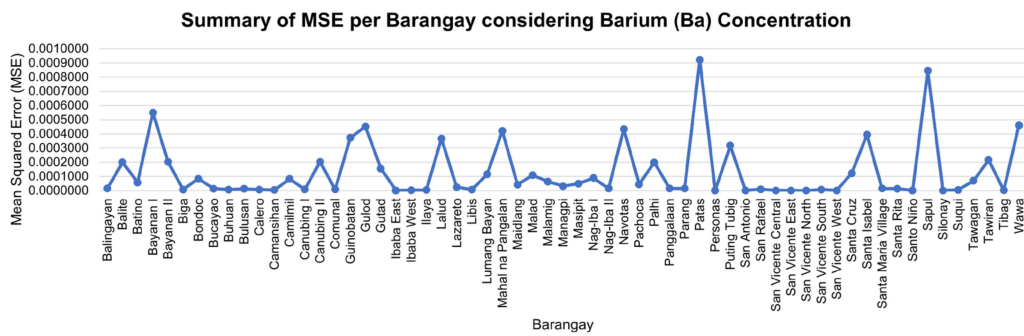
(a)
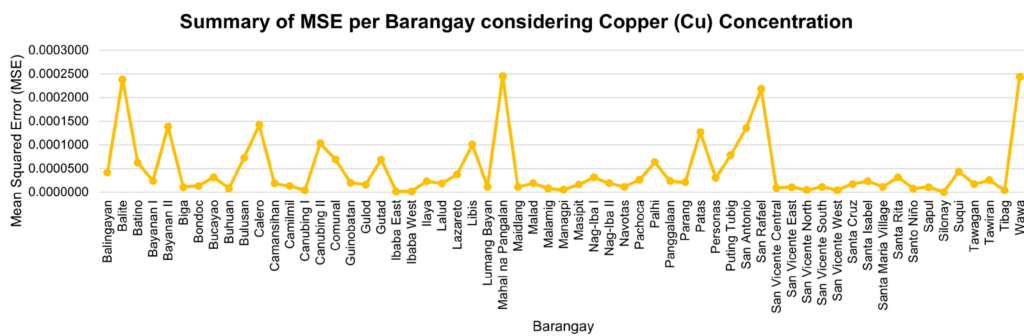
(b)
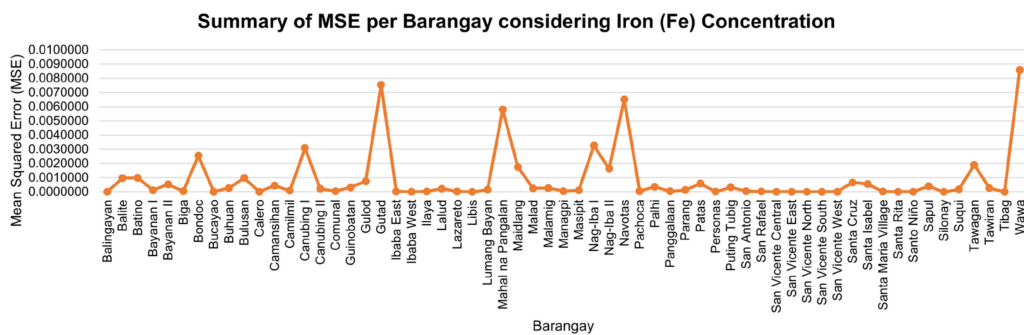
(c)
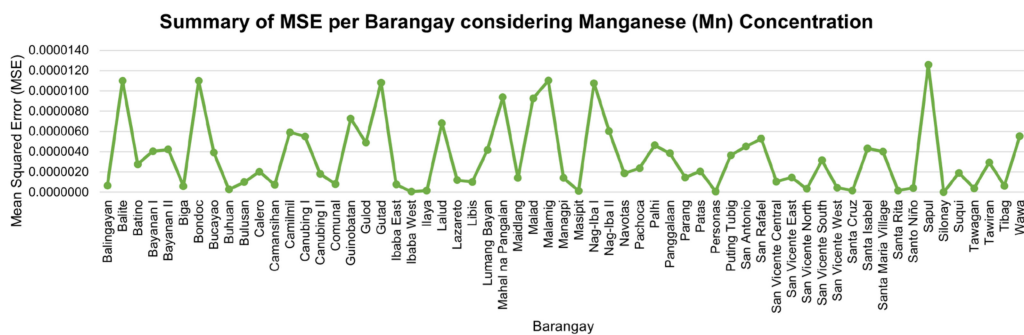
(d)

Figure 14. *Cont.*
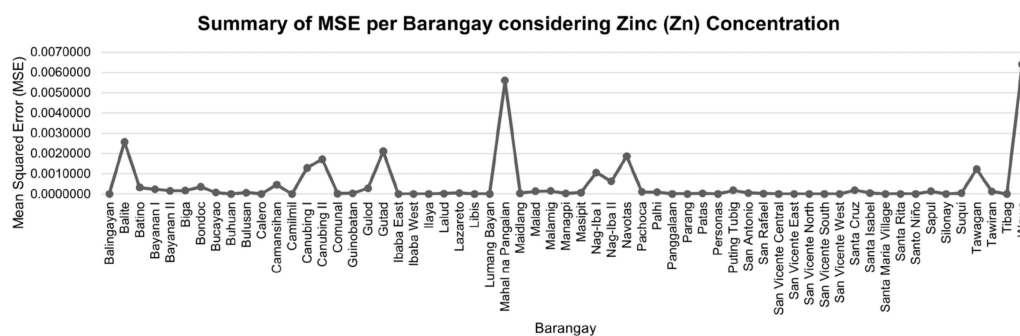
(e)

Figure 14. Summary of MSE per Barangay considering (**a**) Ba, (**b**) Cu, (**c**) Fe, (**d**) Mn, and (**e**) Zn.

4. Discussion

Oriental Mindoro, an island province, is vulnerable to GW pollution and degradation due to natural and human activities. Due to structural disadvantages and characteristics such as smaller land area and population, insufficient natural resources, geographical distribution, and other global factors beyond domestic control, a small island economy is less resilient to the threat of GW deterioration and contamination than larger and more diverse economies [70].

Water plays a critical part in achieving the United Nations' Sustainable Development Goals (SDGs). One of the problems that population has been experiencing is ensuring that everyone achieves SDG 6 (clean water and sanitation) which seeks to guarantee universal access to, and sustainable management of water. Continuous data integration and frequent monitoring remain to be critical components to achieving SDG 6 [71]. Hence, creating tools to aid in carrying out GW monitoring is significant. Tools such as the hybrid NN-PSO+EBK in making GW monitoring convenient to researchers and authorities are important.

Various heavy metals were detected at various sampling sites across Calapan City. The mean concentration of these metals in GW remained below the WHO and PNSDW acceptable levels. The recorded in-situ physicochemical characteristics were also compared to the WHO and PNSDW acceptable limits. The average GW temperature observed in the study area was 29.99 °C while the average GW pH observed was 7.69. Both figures are within the permissible range of WHO and PNSDW. One (1) sampling location exhibited pH value exceeding the maximum limit for pH of PNSDW. The average EC for the area of study was 560.36 μS/cm. This is within the permissible limit of the WHO. One (1) sampling location exhibited an EC value exceeding the WHO limit of 1500 μS/cm. The EC observation made in this location was categorized as Type II. The EC greater than 1500 μS/cm but less than 3000 μS/cm implies medium salts enrichment [72]. The average TDS is 277.15 ppm which was below the maximum allowable limit by the PNSDW and WHO. Though, TDS levels did not exceed the permissible limits set by WHO and PNSDW but were substantially lower or higher than the suggested TDS range of 600−1000 impairing palatability. Specifically, data of water samples from Ibaba West recorded TDS of 900. This number is at the high side of the limit which suggested the probability of impaired taste. On the other hand, the TDS concentrations recorded in Balingayan (60), Biga (50), Canubing (50), Comunal (90), Ibaba East Site 1 (160), Managpi (100), Personas (60), and Sta. Rita (40) were all significantly lower than the recommended range (600−1000 ppm) which may result to flat and insipid flavor.

The heavy metals concentration for GW was also observed in the study area. The Fe concentrations detected in multiple locations were above the WHO and PNSDW standards. However, the rest of the heavy metals detected were within the permissible limits. Water with elevated metals concentration has the potential to cause several public health issues. Health risks associated with elevated Fe in GW is probable. Pollutants entering the human body through drinking water have been shown in numerous studies to have detrimental health consequences for consumers. Micronutrients are essential in living organisms; how-

ever, elevated concentration adversely affects public health. Similar case with Mn which is necessary for humans; however, excessive quantities will have negative consequences. Neurological disorders, such as aberrant walking, ataxia, muscle hypotonicity, and a face devoid of lasting emotions, are frequently associated to Mn [64]. Dysfunction of liver was also reported [73]. Furthermore, excess Mn concentration has been demonstrated to produce neurotoxicity in infants receiving parenteral nourishment [74]. Excess Mn has been also linked to a lower level of IQ in children [64].

Meanwhile, asbestos-related cancer is believed to be caused by free radicals, which are produced by iron. Free radicals produced by iron can cause cancer by oxidizing DNA and causing DNA damage [75]. Additionally, elevated levels of Mn and Fe in drinking water have been associated to a decrease in birth weight in term-born infants [76]. Furthermore, since animals' intestinal mucosa is highly porous, the fast absorption into the blood has been attributed to the Ba^{2+} ions which are rapidly absorbed from the gastrointestinal system and lungs. Moreover, it has been observed that Ba poisoning mostly affects the cardiovascular system; nevertheless, renal dysfunction has been documented as well [77].

The use of in-situ and hybrid machine learning—geostatistical methods are an integral part of data integration for GW quality monitoring. The impact of GW contamination in an island province had been a threat to public health especially when GW is used as primary source of domestic, agricultural and industrial water supply. Application of NN-PSO+EBK hybrid technique enables the establishment of spatial variability map of the contaminants that contributes to the depletion of GW quality. As a result, future undesired consequences could be avoided using this monitoring technique. The NN-PSO+EBK can offer periodic and long-term data that can be utilized for permanent monitoring of GW quality and risk assessments. Also, this tool can be utilized as early warning of GW quality for detrimental effects [78] by human activities and/or natural weathering.

5. Conclusions

An in-situ approach and hybrid MLGI, i.e., NN-PSO+EBK, was applied to assess and evaluate the GW quality in Calapan City, Oriental Mindoro, Philippines. Physicochemical characteristics and metals concentrations were detected onsite at various sampling locations. Generally, the physicochemical analysis of GW samples met the WHO and PNSDW guidelines. The average values for temperature, pH, EC, and TDS were within the permissible limits though few sampling locations exceeded the permissible limits of WHO and PNSDW. The pH of all samples was within the limits set by the PNSDW. Barangays Buhuan, Camansihan, Gutad, Ibaba East (Site 2), Ibaba West, Ilaya, Lazareto, Maidlang, Masipit, Nag-iba II, Pachoca, Parang, San Vicente East, Sta. Cruz, and Sto. Nino recorded elevated EC values. This was attributed to the addition of leachable salts. Also, the recorded TDS values suggested probable impaired palatability by having values significantly below the recommended range of 600−1000 ppm. Heavy metals analysis showed that only Fe detected in multiple GW samples had concentration above the WHO and PNSDW maximum permitted levels. This condition presents health concerns to the consumers. The record on Fe concentration in Brgy. Gutad GW samples were above WHO and PNSDW limit. Other GW samples recorded target metals concentration within the WHO and PNSDW permissible limits. The spot sampling analysis results showed that the generated maps by hybrid technique such as NN-PSO+EBK were reliable in describing the heavy metal concentration in the city of Calapan based on its MSE, R and AIC values.

This study is useful as a reference to providing techniques on gathering data for GW quality monitoring to help attain SDGs 6. It is suggested to conduct a study targeting other metals and regular monitoring of its concentration using this hybrid MLGI technique. Additionally, the regular monitoring is necessary to better understanding of the possible health consequences. Furthermore, a health risk assessment based on GW quality should be conducted. Another, preliminary interventions on GW quality control is necessary.

Appendix A

Table A1. Observed Physicochemical Properties of Groundwater Samples.

Sampling No.	Barangay	Latitude	Longitude	Temp (°C)	pH	EC (µS/cm)	TDS (ppm)
1	Balingayan (Site 1)	13.31903° N	121.13432° E	28.3	7.9	130	60
2	Balingayan (Site 2)	13.32454° N	121.13555° E	28.5	8.4	130	60
3	Biga	13.32791° N	121.17312° E	26.2	8.5	120	50
4	Buhuan	13.31451° N	121.22395°E	29.2	7.6	660	320
5	Camansihan	13.33399° N	121.22656° E	30.7	7.8	1200	590
6	Canubing I	13.35590° N	121.14091° E	27.1	8.8	130	50
7	Comunal	13.31267° N	121.16494° E	27.2	7.9	200	90
8	Gutad	13.35518° N	121.25278° E	32.4	7.1	900	440
9	Ibaba East (Site 1)	13.41517° N	121.17836° E	31.6	7.5	350	160
10	Ibaba East (Site 2)	13.41484° N	121.17769° E	32.5	7.5	970	480
11	Ibaba West	13.41478° N	121.17676° E	31.4	7.4	1820	900
12	Ilaya	13.41181° N	121.18548° E	31.1	7.1	780	380
13	Lazareto	13.42972° N	121.19940° E	31	7	990	490
14	Maidlang	13.39711° N	121.22727° E	32	7.5	600	290
15	Managpi	13.32512° N	121.19595° E	28.1	7.5	220	100
16	Masipit	13.38917° N	121.16190° E	31.5	7.3	570	270
17	Nag-iba II	13.34643° N	121.25301° E	30.6	7.3	820	400
18	Pachoca	13.41061° N	121.16840° E	29.2	8.1	690	340
19	Palhi	13.37502° N	121.20703° E	30.2	7.4	410	200
20	Panggalaan	13.30148° N	121.19908° E	30.1	7.6	140	160
21	Panggalaan	13.30027° N	121.20041° E	28.4	8.3	180	150
22	Parang	13.40059° N	121.21769° E	33.6	7.7	910	450
23	Personas (Site 1)	13.30623° N	121.14083° E	28.7	8.3	140	60
24	Personas (Site 2)	13.30930° N	121.13945° E	27.4	8.4	140	60
25	San Vicente East	13.31045° N	121.17980° E	32.9	7.6	750	370
26	Sta. Cruz	13.31633° N	121.23461° E	29.7	7.3	500	240
27	Sta. Rita	13.35212° N	121.13091° E	29.7	7.7	100	40
28	Sto. Nino	13.40712° N	121.18545° E	30.3	6.7	1140	560

Appendix B

Figure A1. R Value Plots for Validation and Testing Phase of the NN-PSO: (**a**) Temperature; (**b**) pH; (**c**) EC; (**d**) TDS; (**e**) Ba; (**f**) Cu; (**g**) Fe; (**h**) Mn; (**i**) Zn.

Appendix C

Table A2. Spot Sampling Results in each Barangay of Calapan City.

Brgy. No.	Barangay	Latitude	Longitude	Elev. (m)	Average MSE				
					Ba	Cu	Fe	Mn	Zn
1	Balingayan	13.3241° N	121.1407° E	13.2	0.0000151	0.0000412	0.0000104	0.0000007	0.0000138
2	Balite	13.4131° N	121.1580° E	7.6	0.0002007	0.0002381	0.0009690	0.0000110	0.0025765
3	Batino	13.3494° N	121.2201° E	7.8	0.0000578	0.0000624	0.0009873	0.0000028	0.0003248
4	Bayanan I	13.3679° N	121.1685° E	8.8	0.0005507	0.0000240	0.0001122	0.0000040	0.0002384
5	Bayanan II	13.3560° N	121.1699° E	12.5	0.0002042	0.0001388	0.0005354	0.0000042	0.0001622
6	Biga	13.3270° N	121.1733° E	14.1	0.0000080	0.0000108	0.0000396	0.0000006	0.0001686
7	Bondoc	13.3867° N	121.2010° E	165.5	0.0000844	0.0000133	0.0025490	0.0000110	0.0003627
8	Bucayao	13.3066° N	121.1915° E	17.3	0.0000146	0.0000316	0.0000047	0.0000039	0.0000776
9	Buhuan	13.3106° N	121.1915° E	12.8	0.0000069	0.0000081	0.0002698	0.0000003	0.0000034
10	Bulusan	13.4037° N	121.2012° E	28.4	0.0000127	0.0000730	0.0009766	0.0000010	0.0000702
11	Calero	13.4159° N	121.1831° E	9.4	0.0000079	0.0001424	0.0000126	0.0000020	0.0000081
12	Camansihan	13.3428° N	121.2290° E	7.1	0.0000042	0.0000183	0.0004483	0.0000007	0.0004709
13	Camilmil	13.4061° N	121.1760° E	8.4	0.0000827	0.0000129	0.0000828	0.0000059	0.0000046
14	Canubing I	13.3554° N	121.1423° E	8.6	0.0000088	0.0000043	0.0030914	0.0000055	0.0012961
15	Canubing II	13.3261° N	121.1216° E	12.9	0.0002042	0.0001033	0.0002191	0.0000018	0.0017159
16	Comunal	13.3075° N	121.1606° E	19.5	0.0000085	0.0000694	0.0000558	0.0000008	0.0000270
17	Guinobatan	13.3829° N	121.1818° E	9.7	0.0003723	0.0000199	0.0003131	0.0000073	0.0000374
18	Gulod	13.3433° N	121.2073° E	9.0	0.0004521	0.0000160	0.0007486	0.0000049	0.0002808
19	Gutad	13.3597° N	121.2464° E	7.2	0.0001561	0.0000687	0.0075550	0.0000108	0.0021064
20	Ibaba East	13.4149° N	121.1788° E	6.6	0.0000009	0.0000016	0.0000250	0.0000008	0.0000022
21	Ibaba West	13.4146° N	121.1762° E	5.9	0.0000027	0.0000018	0.0000010	0.0000001	0.0000021
22	Ilaya	13.4129° N	121.1840° E	8.7	0.0000040	0.0000232	0.0000372	0.0000002	0.0000020
23	Lalud	13.3993° N	121.1739° E	9.1	0.0003669	0.0000186	0.0002229	0.0000068	0.0000209
24	Lazareto	13.4286° N	121.1995° E	12.9	0.0000251	0.0000371	0.0000305	0.0000012	0.0000589
25	Libis	13.4149° N	121.1847° E	9.2	0.0000074	0.0001006	0.0000018	0.0000010	0.0000036
26	Lumang Bayan	13.4009° N	121.1816° E	6.8	0.0001156	0.0000113	0.0001495	0.0000042	0.0000077
27	Mahal na Pangalan	13.4082° N	121.1502° E	9.0	0.0004217	0.0002451	0.0057978	0.0000094	0.0056021
28	Maidlang	13.3883° N	121.2339° E	8.3	0.0000427	0.0000111	0.0017492	0.0000014	0.0000401
29	Malad	13.3396° N	121.1588° E	10.8	0.0001085	0.0000189	0.0002558	0.0000093	0.0001421
30	Malamig	13.3439° N	121.1456° E	10.7	0.0000640	0.0000077	0.0002769	0.0000110	0.0001567
31	Managpi	13.3282° N	121.1997° E	18.0	0.0000321	0.0000051	0.0000465	0.0000014	0.0000330
32	Masipit	13.3869° N	121.1603° E	6.6	0.0000484	0.0000162	0.0001101	0.0000002	0.0000723
33	Nag-Iba I	13.3400° N	121.2721° E	8.5	0.0000893	0.0000313	0.0032634	0.0000108	0.0010670
34	Nag-Iba II	13.3470° N	121.2622° E	11.0	0.0000154	0.0000190	0.0016347	0.0000060	0.0006289
35	Navotas	13.3739° N	121.2486° E	7.5	0.0004349	0.0000114	0.0065142	0.0000019	0.0018669
36	Pachoca	13.4108° N	121.1677° E	6.0	0.0000441	0.0000266	0.0000465	0.0000024	0.0001095
37	Palhi	13.3750° N	121.2070° E	18.6	0.0001992	0.0000633	0.0003630	0.0000046	0.0000934
38	Panggalaan	13.3012° N	121.1990° E	17.9	0.0000164	0.0000234	0.0000402	0.0000039	0.0000126
39	Parang	13.4035° N	121.2182° E	9.5	0.0000148	0.0000209	0.0001279	0.0000015	0.0000127
40	Patas	13.3452° N	121.1222° E	12.9	0.0009213	0.0001269	0.0005874	0.0000021	0.0000333
41	Personas	13.3083° N	121.1438° E	14.5	0.0000006	0.0000300	0.0000213	0.0000001	0.0000028
42	Puting Tubig	13.3470° N	121.1887° E	7.3	0.0003178	0.0000788	0.0003261	0.0000037	0.0001840
43	San Antonio	13.4259° N	121.1956° E	14.0	0.0000013	0.0001353	0.0000519	0.0000045	0.0000587
44	San Rafael	13.4216° N	121.1911° E	6.4	0.0000099	0.0002183	0.0000171	0.0000053	0.0000280
45	San Vicente Central	13.4120° N	121.1787° E	8.6	0.0000010	0.0000086	0.0000024	0.0000011	0.0000011
46	San Vicente East	13.4098° N	121.1798° E	9.3	0.0000009	0.0000106	0.0000044	0.0000014	0.0000004
47	San Vicente North	13.4138° N	121.1785° E	6.7	0.0000003	0.0000045	0.0000005	0.0000003	0.0000001
48	San Vicente South	13.4095° N	121.1779° E	7.6	0.0000072	0.0000115	0.0000123	0.0000031	0.0000018
49	San Vicente West	13.4124° N	121.1765° E	7.8	0.0000005	0.0000040	0.0000024	0.0000005	0.0000010
50	Santa Cruz	13.3169° N	121.2370° E	12.1	0.0001231	0.0000173	0.0006697	0.0000002	0.0001946
51	Santa Isabel	13.3654° N	121.1577° E	5.3	0.0003942	0.0000233	0.0005533	0.0000043	0.0000575
52	Santa Maria Village	13.4093° N	121.1748° E	6.3	0.0000154	0.0000115	0.0000167	0.0000040	0.0000019
53	Santa Rita	13.3489° N	121.1303° E	11.1	0.0000139	0.0000317	0.0000140	0.0000002	0.0000081
54	Santo Niño	13.4066° N	121.1848° E	8.2	0.0000004	0.0000075	0.0000057	0.0000004	0.0000003
55	Sapul	13.3651° N	121.1885° E	14.3	0.0008450	0.0000108	0.0003983	0.0000126	0.0001391
56	Silonay	13.3992° N	121.2248° E	8.8	0.0000004	0.0000004	0.0000011	0.0000000	0.0000007
57	Suqui	13.4177° N	121.2040° E	11.1	0.0000057	0.0000434	0.0001749	0.0000019	0.0000464
58	Tawagan	13.3712° N	121.1448° E	8.6	0.0000693	0.0000169	0.0019052	0.0000004	0.0012349
59	Tawiran	13.3950° N	121.1680° E	7.0	0.0002160	0.0000253	0.0002604	0.0000030	0.0001365
60	Tibag	13.4123° N	121.1730° E	8.2	0.0000018	0.0000040	0.0000027	0.0000006	0.0000014
61	Wawa	13.4025° N	121.1453° E	8.8	0.0004609	0.0002441	0.0085841	0.0000055	0.0063922

References

1.　Pineda-Pineda, J.J.; Martínez-Martínez, C.T.; Méndez-Bermúdez, J.A.; Muñoz-Rojas, J.; Sigarreta, J.M. Application of Bipartite Networks to the Study of Water Quality. *Sustainability* **2020**, *12*, 5143. [CrossRef]
2.　Mekonnen, M.M.; Hoekstra, A.Y. Four billion people facing severe water scarcity. *Sci. Adv.* **2016**, *2*, e1500323. [CrossRef]
3.　Jha, M.K.; Shekhar, A.; Jenifer, M.A. Assessing groundwater quality for drinking water supply using hybrid fuzzy-GIS-based water quality index. *Water Res.* **2020**, *179*, 115867. [CrossRef] [PubMed]
4.　Department of Environment and Natural Resources—Mines and Geosciences Bureau. Geohazard Maps. Available online: http://www.region4b.mgb.gov.ph/28-geohazard-maps/98-geohazard-maps (accessed on 25 October 2021).
5.　Philippine Statistics Authority. Compendium of Philippine Environment Statistics Component 2: Environmental Resources and their Use. Available online: https://psa.gov.ph/press-releases/id/163678 (accessed on 25 October 2021).
6.　Kumar, A.; Cabral-Pinto, M.; Kumar, A.; Kumar, M.; Dinis, P.A. Estimation of Risk to the Eco-Environment and Human Health of Using Heavy Metals in the Uttarakhand Himalaya, India. *Appl. Sci.* **2020**, *10*, 7078. [CrossRef]
7.　Kumar, A.; Jigyasu, D.K.; Kumar, A.; Subrahmanyam, G.; Mondal, R.; Shabnam, A.A.; Cabral-Pinto, M.M.S.; Malyan, S.K.; Chaturvedi, A.K.; Gupta, D.K.; et al. Nickel in terrestrial biota: Comprehensive review on contamination, toxicity, tolerance and its remediation approaches. *Chemosphere* **2021**, *275*, 129996. [CrossRef] [PubMed]
8.　Kumar, A.; Cabral Pinto, M.; Candeias, C.; Dinis, P.A. Baseline maps of potentially toxic elements in the soil of Garhwal Himalayas, India: Assessment of their eco-environmental and human health risks. *Land Degrad. Dev.* **2021**, *10*, 3984. [CrossRef]
9.　Hartzler, D.A.; Jain, J.C.; McIntyre, D.L. Development of a subsurface LIBS sensor for in situ groundwater quality monitoring with applications in CO 2 leak sensing in carbon sequestration. *Sci. Rep.* **2019**, *9*, 1–10.
10.　Bu, X.; Koide, K.; Carder, E.J.; Welch, C.J. Rapid analysis of residual palladium in pharmaceutical development using a catalysis-based fluorometric method. *Org. Process Res. Dev.* **2013**, *17*, 108–113. [CrossRef]
11.　Farghaly, O.A.; Hameed, R.A.; Abu-Nawwas, A.A.H. Analytical application using modern electrochemical techniques. *Int. J. Electrochem. Sci.* **2014**, *9*, 3287–3318.
12.　Kudr, J.; Richtera, L.; Nejdl, L.; Xhaxhiu, K.; Vitek, P.; Rutkay-Nedecky, B.; Hynek, D.; Kopel, P.; Adam, V.; Kizek, R. Improved electrochemical detection of zinc ions using electrode modified with electrochemically reduced graphene oxide. *Materials* **2016**, *9*, 31. [CrossRef]
13.　Estela, J.M.; Tomás, C.; Cladera, A.; Cerda, V. Potentiometric stripping analysis: A review. *Crit. Rev. Anal. Chem.* **1995**, *25*, 91–141. [CrossRef]
14.　Khadro, B.; Sikora, A.; Loir, A.S.; Errachid, A.; Garrelie, F.; Donnet, C.; Jaffrezic-Renault, N. Electrochemical performances of B doped and undoped diamond-like carbon (DLC) films deposited by femtosecond pulsed laser ablation for heavy metal detection using square wave anodic stripping voltammetric (SWASV) technique. *Sens. Actuators B Chem.* **2011**, *155*, 120–125. [CrossRef]
15.　Avuthu, S.G.R.; Narakathu, B.B.; Eshkeiti, A.; Emamian, S.; Bazuin, B.J.; Joyce, M.; Atashbar, M.Z. Detection of heavy metals using fully printed three electrode electrochemical sensor. In *SENSORS*; IEEE: New York, NY, USA, 2014; pp. 669–672.
16.　Cheng, L.; Liu, X.; Lei, J.; Ju, H. Low-potential electrochemiluminescent sensing based on surface unpassivation of CdTe quantum dots and competition of analyte cation to stabilizer. *Anal. Chem.* **2010**, *82*, 3359–3364. [CrossRef] [PubMed]
17.　Bansod, B.; Kumar, T.; Thakur, R.; Rana, S.; Singh, I. A review on various electrochemical techniques for heavy metal ions detection with different sensing platforms. *Biosens. Bioelectron.* **2017**, *94*, 443–455. [CrossRef]
18.　Borgese, L.; Zacco, A.; Bontempi, E.; Pellegatta, M.; Vigna, L.; Patrini, L.; Riboldi, L.; Rubino, F.M.; Depero, L.E. Use of total reflection X-ray fluorescence (TXRF) for the evaluation of heavy metal poisoning due to the improper use of a traditional ayurvedic drug. *J. Pharm. Biomed. Anal.* **2010**, *52*, 787–790. [CrossRef]
19.　De Jesus, K.; Senoro, D.B.; Dela Cruz, J.C.; Chan, E.B. A Hybrid Neural Network—Particle Swarm Optimization In-formed Spatial Interpolation Technique for Groundwater Quality Mapping in a Small Island Province of the Philippines. *Toxics* **2021**, *9*, 273. [CrossRef] [PubMed]
20.　El-Rawy, M.; Fathi, H.; Abdalla, F. Integration of remote sensing data and in situ measurements to monitor the water quality of the Ismailia Canal, Nile Delta, Egypt. *Environ. Geochem. Health* **2020**, *42*, 2101–2120. [CrossRef] [PubMed]
21.　Solis, K.L.B.; Macasieb, R.Q.; Parangat, R.C.; Resurreccion, A.C.; Ocon, J.D. Spatiotemporal Variation of Groundwater Arsenic in Pampanga, Philippines. *Water* **2020**, *12*, 2366. [CrossRef]
22.　Tiankao, W.; Chotpantarat, S. Risk assessment of arsenic from contaminated soils to shallow groundwater in Ong Phra Sub-District, Suphan Buri Province, Thailand. *J. Hydrol. Reg. Stud.* **2018**, *19*, 80–96. [CrossRef]
23.　Mogaji, K.A. Application of vulnerability modeling techniques in groundwater resources management: A comparative study. *Appl. Water Sci.* **2018**, *8*, 1–24. [CrossRef]
24.　Nistor, M.M.; Rahardjo, H.; Satyanaga, A.; Hao, K.Z.; Xiaosheng, Q.; Sham, A.W.L. Investigation of groundwater table distribution using borehole piezometer data interpolation: Case study of Singapore. *Eng. Geol.* **2020**, *271*, 105590. [CrossRef]
25.　Rusydi, A.F.; Onodera, S.I.; Saito, M.; Ioka, S.; Maria, R.; Ridwansyah, I.; Delinom, R.M. Vulnerability of groundwater to iron and manganese contamination in the coastal alluvial plain of a developing Indonesian city. *SN Appl. Sci.* **2021**, *3*, 1–12. [CrossRef]
26.　Lado, L.R.; Polya, D.; Winkel, L.; Berg, M.; Hegan, A. Modelling arsenic hazard in Cambodia: A geostatistical approach using ancillary data. *Appl. Geochem.* **2008**, *23*, 3010–3018. [CrossRef]
27.　Viossanges, M.; Pavelic, P.; Rebelo, L.M.; Lacombe, G.; Sotoukee, T. Regional mapping of groundwater resources in data-scarce regions: The case of Laos. *Hydrology* **2018**, *5*, 2. [CrossRef]

28. Giang, P.Q.; Nakhapakorn, K.; Ussawarujikulchai, A. Effectiveness of different spatial interpolators in estimating heavy metal contamination in shallow groundwater: A case study of arsenic contamination in Hanoi, Vietnam. *Environ. Nat. Resour. J.* **2011**, *9*, 31–37.

29. Agutaya, C.A.C.; Zamora, J.T. Developmental Projects in Calapan City, Philippines: Localization Perspectives. *Am. J. Educ. Res.* **2018**, *6*, 133–136.

30. United States Environmental Protection Agency (U.S. E.P.A). *Operating Procedure for In Situ Water Quality Monitoring (SESDPROC-111-R4)*. Available online: https://www.epa.gov/sites/default/files/2015-06/documents/Insitu-Water-Quality-Mon.pdf (accessed on 16 December 2021).

31. Hanna Instruments. HI9811-5 Portable pH/EC/TDS/Temperature. Available online: https://www.hannainst.com/portable-ph-ec-tds-temperature-meter-hi9811-5.html (accessed on 16 December 2021).

32. Magalona, M.L.; Peralta, M.M.; Lacsamana, M.S.; Sabularse, V.C.; Pelegrina, A.B.; De Guzman, C.C. Analysis of Inorganic Arsenic (As (III) and Total As) and Some Physicochemical Parameters in Groundwater Samples from Selected Areas in Bulacan, Batangas, and Laguna, Philippines. *KIMIKA* **2019**, *30*, 28–38. [CrossRef]

33. Groover, K.D.; Izbicki, J.A. Elemental analysis using a handheld X-ray fluorescence spectrometer (No. 2016-3043). *U.S. Geol. Surv. Fact Sheet* **2016**, 2015–3043. [CrossRef]

34. Analytical Methods Committee AMCTB No. 89. Hand-held X-ray fluorescence spectrometry. *Anal. Methods* **2019**, *11*, 2498–2501. [CrossRef]

35. Muramatsu, Y.; Izawa, R.; Nishioka, H.; Nogami, T. X-ray fluorescence analysis of dilute heavy-metals in water using a portable x-ray fluorescence spectrometer with the metal-adsorbent, tobermorite. *X-sen Bunseki No Shinpo* **2009**, *40*, 195–201.

36. Pearson, D.; Weindorf, D.C.; Chakraborty, S.; Li, B.; Koch, J.; Van Deventer, P.; de Wet, J.; Kusi, N.Y. Analysis of metal-laden water via portable X-ray fluorescence spectrometry. *J. Hydrol.* **2018**, *561*, 267–276. [CrossRef]

37. Zhou, S.; Yuan, Z.; Cheng, Q.; Zhang, Z.; Yang, J. Rapid in situ determination of heavy metal concentrations in polluted water via portable XRF: Using Cu and Pb as example. *Environ. Pollut.* **2018**, *243*, 1325–1333. [CrossRef]

38. Pearson, D.; Chakraborty, S.; Duda, B.; Li, B.; Weindorf, D.C.; Deb, S.; Brevik, E.; Ray, D.P. Water analysis via portable X-ray fluorescence spectrometry. *J. Hydrol.* **2017**, *544*, 172–179. [CrossRef]

39. Crocombe, R.A.; Leary, P.E.; Kammrath, B.W. *Portable Spectroscopy and Spectrometry, Applications*; John Wiley & Sons: Hoboken, NJ, USA, 2021; Volume 2, ISBN 978-111-963-640-3.

40. Magesh, N.S.; Chandrasekar, N.; Elango, L. Occurrence and distribution of fluoride in the groundwater of the Tamiraparani River basin, South India: A geostatistical modeling approach. *Environ. Earth Sci.* **2016**, *75*, 1–16. [CrossRef]

41. Shariati, M.; Mafipour, M.S.; Mehrabi, P.; Bahadori, A.; Zandi, Y.; Salih, M.N.; Nguyen, H.; Dou, J.; Song, X.; Poi-Ngian, S. Application of a hybrid artificial neural network-particle swarm optimization (ANN-PSO) model in behavior prediction of channel shear connectors embedded in normal and high-strength concrete. *Appl. Sci.* **2019**, *9*, 5534. [CrossRef]

42. Kayabasi, E.; Ozturk, S.; Celik, E.; Kurt, H. Determination of cutting parameters for silicon wafer with a Diamond Wire Saw using an artificial neural network. *Sol. Energy* **2017**, *149*, 285–293. [CrossRef]

43. Ozturk, S.; Kayabasi, E.; Celik, E.; Kurt, H. Determination of lapping parameters for silicon wafer using an artificial neural network. *J. Mater. Sci.: Mater. Electron.* **2018**, *29*, 260–270. [CrossRef]

44. Lin, Y.H.; Hu, Y.C. Electrical energy management based on a hybrid artificial neural network-particle swarm optimization-integrated two-stage non-intrusive load monitoring process in smart homes. *Processes* **2018**, *6*, 236. [CrossRef]

45. World Health Organization. *Guidelines for Drinking-Water Quality*, 3rd ed.; World Health Organization: Geneva, Switzerland, 2004; Volume 1, ISBN 92-4-154638-7.

46. Department of Health—Food and Drug Administration. Administrative Order No. 2017-0010—Philippine National Standards for Drinking Water of 2017. Available online: https://www.fda.gov.ph/administrative-order-no-2017-0010-philippine-national-standards-for-drinking-water-of-2017 (accessed on 25 October 2021).

47. Li, H.; Shi, A.; Li, M.; Zhang, X. Effect of pH, temperature, dissolved oxygen, and flow rate of overlying water on heavy metals release from storm sewer sediments. *J. Chem.* **2013**, *2013*, 434012. [CrossRef]

48. Zhu, K.; Blum, P.; Ferguson, G.; Balke, K.D.; Bayer, P. The geothermal potential of urban heat islands. *Environ. Res. Lett.* **2010**, *5*, 044002. [CrossRef]

49. Lomboy, M.; Riego de Dios, J.; Magtibay, B.; Quizon, R.; Molina, V.; Fadrilan-Camacho, V.; See, J.; Enoveso, A.; Barbosa, L.; Agravante, A. Updating national standards for drinking-water: A Philippine experience. *J. Water Health* **2017**, *15*, 288–295. [CrossRef] [PubMed]

50. Edwards, K.A.; Classen, G.A.; Schroten, E.H.J. The Water Resource in Tropical Africa and Its Exploitation. Available online: https://www.ilri.org/publications/water-resource-tropical-africa-and-its-exploitation (accessed on 20 November 2021).

51. Anyanwu, B.O.; Ezejiofor, A.N.; Igweze, Z.N.; Orisakwe, O.E. Heavy metal mixture exposure and effects in developing nations: An update. *Toxics* **2018**, *6*, 65. [CrossRef]

52. Fenton, T.R.; Huang, T. Systematic review of the association between dietary acid load, alkaline water and cancer. *BMJ open* **2016**, *6*, e010438. [CrossRef] [PubMed]

53. Jan, A.T.; Azam, M.; Siddiqui, K.; Ali, A.; Choi, I.; Haq, Q.M. Heavy metals and human health: Mechanistic insight into toxicity and counter defense system of antioxidants. *Int. J. Mol. Sci.* **2015**, *16*, 29592–29630. [CrossRef]

54. Patil, V.T.; Patil, P.R. Physicochemical Analysis of Selected Groundwater Samples of Amalner Town in Jalgaon District, Maharashtra, India. *E-J. Chem.* **2010**, *7*, 111–116. [CrossRef]

55. Oyem, H.H.; Oyem, I.M.; Ezeweali, D. Temperature, pH, electrical conductivity, total dissolved solids and chemical oxygen demand of groundwater in Boji-BojiAgbor/Owa area and immediate suburbs. *Res. J. Environ. Sci.* **2014**, *8*, 444. [CrossRef]

56. Ramasamy, S. Barium in Drinking Water—Background document for development of WHO Guidelines for Drinking-water Quality. Available online: https://www.who.int/water_sanitation_health/water-quality/guidelines/chemicals/barium-background-jan17.pdf (accessed on 26 October 2021).

57. Kroschwitz, J.I.; Howe-Grant, M. *Kirk-Othmer Encyclopedia of Chemical Technology*, 3rd ed.; Grayson, M., Eckroth, D., Eds.; John Wiley and Sons: New York, NY, USA, 1978; Volume 3, pp. 457–463.

58. Miner, S. *Air Pollution Aspects of Barium and Its Compounds*; Contract No. Ph-22-68-25; Litton Systems, Inc.: Bethesda, MD, USA, 1969; p. 69.

59. Pinto, V.M.; Hartmann, L.A. Flow-by-flow chemical stratigraphy and evolution of thirteen Serra Geral Group basalt flows from Vista Alegre, southernmost Brazil. *An. Acad. Bras. Cienc.* **2011**, *83*, 425–440. [CrossRef]

60. Vieira, I.F.B.; Rolim Neto, F.C.; Carvalho, M.N.; Caldas, A.M.; Costa, R.C.A.; Silva, K.S.D.; Parahyba, R.D.B.V.; Pacheco, F.A.L.; Fernendes, L.F.S.; Pissarra, T.C.T. Water Security Assessment of Groundwater Quality in an Anthropized Rural Area from the Atlantic Forest Biome in Brazil. *Water* **2020**, *12*, 623. [CrossRef]

61. Beyene, G.; Aberra, D.; Fufa, F. Evaluation of the suitability of groundwater for drinking and irrigation purposes in Jimma Zone of Oromia, Ethiopia. *Groundw. Sustain. Dev.* **2019**, *9*, 100216. [CrossRef]

62. Carasek, F.L.; Baldissera, R.; Oliveira, J.V.; Scheibe, L.F.; Dal Magro, J. Quality of the groundwater of the Serra Geral aquifer system of Santa Catarina west region, Brazil. *Groundw. Sustain. Dev.* **2020**, *10*, 100346. [CrossRef]

63. Maher, K. The dependence of chemical weathering rates on fluid residence time. *Earth Planet. Sci. Lett.* **2010**, *294*, 101–110. [CrossRef]

64. Sholehhudin, M.; Azizah, R.; Sham, A.S.S.M.; Amiruddin, Z. Analysis of Heavy Metals (Cadmium, Chromium, Lead, Manganese, and Zinc) in Well Water in East Java Province, Indonesia. *Malays. J. Med. Health Sci.* **2021**, *17*, 146–153.

65. Zhang, Z.; Xiao, C.; Adeyeye, O.; Yang, W.; Liang, X. Source and mobilization mechanism of iron, manganese and arsenic in groundwater of Shuangliao City, Northeast China. *Water* **2020**, *12*, 534. [CrossRef]

66. Abou Zakhem, B.; Al-Charideh, A.; Kattaa, B. Using principal component analysis in the investigation of groundwater hydrochemistry of Upper Jezireh Basin, Syria. *Hydrol. Sci. J.* **2017**, *62*, 2266–2279.

67. Sunkari, E.D.; Abu, M. Hydrochemistry with special reference to fluoride contamination in groundwater of the Bongo District, Upper East Region, Ghana. *Sustain. Water. Resour. Manag.* **2019**, *5*, 1803–1814. [CrossRef]

68. Wali, S.U.; Alias, N.; Harun, S.B. Reevaluating the hydrochemistry of groundwater in basement complex aquifers of Kaduna Basin, NW Nigeria using multivariate statistical analysis. *Environ. Earth Sci.* **2021**, *80*, 1–25. [CrossRef]

69. Senoro, D.B.; De Jesus, K.L.M.; Yanuaria, C.A.; Bonifacio, P.B.; Manuel, M.T.; Wang, B.N.; Kao, C.C.; Wu, T.N.; Ney, F.P.; Natal, P. Rapid site assessment in a small island of the Philippines contaminated with mine tailings using ground and areal technique: The environmental quality after twenty years. In *IOP Conference Series: Earth and Environmental Science*; IOP Publishing: Bristol, UK, 2019; Volume 351, p. 012022.

70. Wright, N. Small Island Developing States, disaster risk management, disaster risk reduction, climate change adaptation and tourism. *Background Paper for the Global Assessment Report on DRR 2013*. 2013. Available online: https://www.preventionweb.net/english/hyogo/gar/2013/en/bgdocs/Wright,%20N.,%202013.pdf (accessed on 20 November 2021).

71. Lopez-Maldonado, Y.; Batllori-Sampedro, E.; Binder, C.R.; Fath, B.D. Local groundwater balance model: Stakeholders' efforts to address groundwater monitoring and literacy. *Hydrol. Sci. J.* **2017**, *62*, 2297–2312. [CrossRef]

72. Galhardi, J.A.; Bonotto, D.M. Hydrogeochemical features of surface water and groundwater contaminated with acid mine drainage (AMD) in coal mining areas: A case study in southern Brazil. *Environ. Sci. Pollut.* **2016**, *23*, 18911–18927.

73. Williams, M.; Todd, G.D.; Roney, N.; Crawford, J.; Coles, C.; McClure, P.R.; Garey, J.D.; Zaccaria, K.; Citra, M. *Toxicological Profile for Manganese*; Agency for Toxic Substances and Disease Registry (US): Atlanta, GA, USA, 2012.

74. Erikson, K.M.; Thompson, K.; Aschner, J.; Aschner, M. Manganese neurotoxicity: A focus on the neonate. *Pharmacol. Ther.* **2007**, *113*, 369–377. [CrossRef]

75. Bhasin, G.; Kauser, H.; Athar, M. Iron augments stage-I and stage-II tumor promotion in murine skin. *Cancer Lett.* **2002**, *183*, 113–122. [CrossRef]

76. Grazuleviciene, R.; Nadisauskiene, R.; Buinauskiene, J.; Grazulevicius, T. Effects of elevated levels of manganese and iron in drinking water on birth outcomes. *Pol. J. Environ. Stud.* **2009**, *18*, 819–825.

77. Kravchenko, J.; Darrah, T.H.; Miller, R.K.; Lyerly, H.K.; Vengosh, A. A review of the health impacts of barium from natural and anthropogenic exposure. *Environ. Geochem. Health* **2014**, *36*, 797–814. [CrossRef] [PubMed]

78. MacDonald, A.M.; Bonsor, H.C.; Ahmed, K.M.; Burgess, W.G.; Basharat, M.; Calow, R.C.; Dixit, A.; Foster, S.S.D.; Gopal, K.; Lapworth, D.J.; et al. Groundwater quality and depletion in the Indo-Gangetic Basin mapped from in situ observations. *Nat. Geosci.* **2016**, *9*, 762–766. [CrossRef]